Journal of Computational Physics 369 (2018) 1–15

Contents lists available at ScienceDirect

Journal of Computational Physics

www.elsevier.com/locate/jcp

Numerical solution of an inverse boundary value problem for the heat equation with unknown inclusions

Haibing Wang*, Yi Li

School of Mathematics, Southeast University, Nanjing 210096, PR China

ARTICLE INFO

Article history:
Received 1 August 2017
Received in revised form 3 February 2018
Accepted 4 May 2018
Available online 9 May 2018

Keywords:
Inverse problem
Unknown inclusions
Heat equation
Layer potential

ABSTRACT

We consider the problem of reconstructing unknown inclusions inside a thermal conductor from boundary measurements, which arises from active thermography and is formulated as an inverse boundary value problem for the heat equation. In our previous works, we proposed a sampling-type method for reconstructing the boundary of the unknown inclusion and gave its rigorous mathematical justification. In this paper, we continue our previous works and provide a further investigation of the reconstruction method from both the theoretical and numerical points of view. First, we analyze the solvability of the Neumann-to-Dirichlet map gap equation and establish a relation of its solution to the Green function of an interior transmission problem for the inclusion. This naturally provides a way of computing this Green function from the Neumann-to-Dirichlet map. Our new findings reveal the essence of the reconstruction method. A convergence result for noisy measurement data is also proved. Second, based on the heat layer potential argument, we perform a numerical implementation of the reconstruction method for the homogeneous inclusion case. Numerical results are presented to show the efficiency and stability of the proposed method.

1. Introduction

Consider the heat conduction in a two-layered medium (Fig. 1.1). Denote by D_0 and D the outer and inner layers, respectively. Set $\Omega = \overline{D} \cup D_0$. Suppose that the thermal conductivities of D_0 and D are 1 and k, respectively. We also assume that the boundaries ∂D_0 and ∂D of D_0 and D, respectively, are of class C^2. For simplicity of notations, throughout this paper we denote $X \times (0, T)$ and $\partial X \times (0, T)$ by X_T and $(\partial X)_T$, respectively, where X is a bounded domain in $\mathbb{R}^2$ and ∂X denotes its boundary. Injecting a heat flux g on $\partial\Omega$ over some time interval $(0, T)$, the temperature distribution u in Ω_T can be modeled by the following initial-boundary value problem:

$$\begin{cases} (\partial_t - \nabla \cdot k\nabla)u = 0 & \text{in } D_T, \\ (\partial_t - \Delta)u = 0 & \text{in } (\Omega \setminus \overline{D})_T, \\ u|_- - u|_+ = 0 & \text{on } (\partial D)_T, \\ k\partial_\nu u|_- - \partial_\nu u|_+ = 0 & \text{on } (\partial D)_T, \\ \partial_\nu u = g & \text{on } (\partial\Omega)_T, \\ u = 0 & \text{at } t = 0, \end{cases} \tag{1.1}$$

* Corresponding author.
E-mail address: hbwang@seu.edu.cn (H. Wang).

https://doi.org/10.1016/j.jcp.2018.05.008
0021-9991/

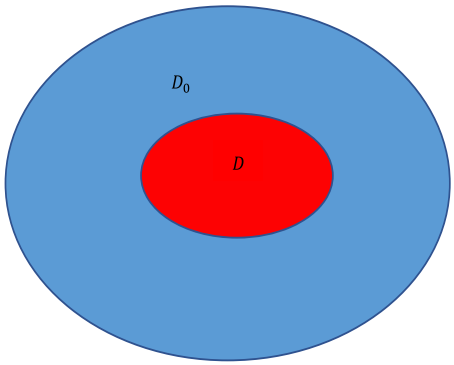

Fig. 1.1. Configuration of the medium.

where ν on ∂D (or $\partial\Omega$) is the unit normal vector directed into the exterior of D (or Ω). Here the subscripts "+" and "−" indicate the trace taken from the exterior and interior of D, respectively.

The above model has many important applications in sciences and engineering. In active thermography, D is regarded as an inclusion and D_0 is the background medium. In this case, the forward problem is to determine the temperature distribution in Ω_T for any injected heat flux g on $(\partial\Omega)_T$, while the inverse problem is to reconstruct the unknown inclusion D from boundary measurements. Instead of recovering the thermal conductivity, we are more interested in finding the location, size and shape of the inclusion as a defect inside the conductor. We proved in [17] that for any $g \in H^{-\frac{1}{2},-\frac{1}{4}}((\partial\Omega)_T)$ there exists a unique solution u to (1.1) in $\tilde{H}^{1,\frac{1}{2}}(\Omega_T)$. Define the Neumann-to-Dirichlet map by

$$\Lambda_D : H^{-\frac{1}{2},-\frac{1}{4}}((\partial\Omega)_T) \to H^{\frac{1}{2},\frac{1}{4}}((\partial\Omega)_T), \quad g \mapsto u|_{(\partial\Omega)_T},$$

which is an idealized measurement data for active thermography. Then our inverse problem is to reconstruct D from Λ_D, where k is unknown. The uniqueness and stability estimate are established in [7,8]. As for reconstruction methods, we refer to [6,9,13–16,21] and the references therein, where the dynamical probe method and the enclosure method are developed. Recently, the authors established a linear sampling-type method for the heat equation in [12,17,18]. However, numerical studies of these reconstruction methods for parabolic inverse boundary value problems are rather limited [19]. Some related works on other kinds of parabolic inverse boundary value problems can be found in [2,3,5,10,11,20].

In this work, based on the heat layer potential theory, we investigate both the forward and inverse problems from the numerical point of view. Especially, the sampling-type reconstruction method established in [17] for our inverse problem will be numerically implemented. Roughly speaking, this reconstruction method is based on the characterization of the solution to the so-called Neumann-to-Dirichlet map gap equation

$$(\Lambda_D - \Lambda_\emptyset)g = G^{\Omega}_{(y,\,s)}(x,\,t), \tag{1.2}$$

where $\Lambda_\emptyset$ is the Neumann-to-Dirichlet map when $D = \emptyset$, and $G^{\Omega}_{(y,\,s)}(x,\,t) := G^{\Omega}(x,\,t;\,y,\,s)$ is the Green function for the heat operator $\partial_t - \Delta$ in Ω_T with homogeneous Neumann boundary condition on $(\partial\Omega)_T$. In terms of this characterization, the norm of the solution to (1.2) serves as an indicator function and the boundary of D can be reconstructed approximately by computing the values of the indicator function at a set of sampling points. Although the sampling-type reconstruction method for inverse scattering problems has been extensively studied; see [1] and the references therein, very few numerical results for parabolic inverse boundary value problems are reported. We recently studied in [19] the numerical implementation of the sampling method for identifying unknown cavities in the thermal conductor, but the rigid inclusion case has not yet considered.

In this paper, we continue our previous works and investigate the numerical realization of the sampling method for parabolic inverse boundary value problems with unknown inclusions. First of all, we supplement the theoretical analysis of our reconstruction method by analyzing the solvability of the equation (1.2) and showing the relation of its solution to the Green function of an associated interior transmission problem. These new findings reveal the essence of the sampling-type reconstruction method. In addition, a convergence result for noisy measurement data is proved. Then, we simulate the measurement data Λ_D by solving the forward problem (1.1), and compute the Neumann-to-Dirichlet map $\Lambda_\emptyset$ and the Green function $G^{\Omega}_{(y,\,s)}(x,\,t)$ by solving the problem (1.1) with $D = \emptyset$. By expressing the solution as a single-layer heat potential, the initial-boundary value problem (1.1) is transformed into a system of boundary integral equations. A numerical scheme for solving the resulting integral equations is introduced. Finally, we solve the discretized Neumann-to-Dirichlet map gap equation using the Tikhonov regularization technique. We show the performance of the reconstruction method from the following two aspects. 1. We test the method for inclusions of different shapes and thermal conductivities. 2. We test the method with short time measurements, namely, using measured data only in a very short time interval. Our numerical results illustrate the efficiency of the reconstruction method.

The rest of this paper is organized as follows. In Section 2, we revisit the sampling-type reconstruction method and show some new theoretical results. In Section 3, we introduce a numerical scheme for solving the forward problem to simulate the measurement for our inverse problem. Two numerical examples are provided in Section 4. Finally, in Section 5, we give some concluding remarks.

2. Reconstruction method for the inverse problem

In this section, we revisit the sampling-type reconstruction method for the heat equation with unknown inclusions studied in [17], and give a further investigation on this method by showing some new theoretical results. Explicitly, we will analyze the solvability of the Neumann-to-Dirichlet map gap equation and explain what is the solution if it does exist. The relation of its solution to the Green function of a related interior transmission problem is established, which reveals the essence of the reconstruction method. For noisy measurement data, a convergence result is also proved.

To begin with, let us introduce the anisotropic Sobolev spaces. For $p, q \geq 0$ we define

$$H^{p,q}(\mathbb{R}^2 \times \mathbb{R}) := L^2(\mathbb{R};\, H^p(\mathbb{R}^2)) \cap H^q(\mathbb{R};\, L^2(\mathbb{R}^2)).$$

For $p, q \leq 0$ we define the space $H^{p,q}$ by duality $H^{p,q}(\mathbb{R}^2 \times \mathbb{R}) := \left(H^{-p,-q}(\mathbb{R}^2 \times \mathbb{R})\right)'$. By $H^{p,q}(X_T)$ we denote the space of restrictions of elements in $H^{p,q}(\mathbb{R}^2 \times \mathbb{R})$ to X_T. The space $H^{p,q}((\partial X)_T)$ is defined analogously. We also define the function spaces

$$\tilde{H}^{1,\frac{1}{2}}(X_T) := \left\{ u \in H^{1,\frac{1}{2}}(X \times (-\infty,\, T)) \,\middle|\, u(x,\, t) = 0 \text{ for } t < 0 \right\},$$
$$\hat{H}^{1,\frac{1}{2}}(X_T) := \left\{ u \in H^{1,\frac{1}{2}}(X \times (0,\, +\infty)) \,\middle|\, u(x,\, t) = 0 \text{ for } t > T \right\},$$
$$\tilde{H}^{1,\frac{1}{2}}(X_T;\, \partial_t - \nabla \cdot \gamma \nabla) := \left\{ u \in \tilde{H}^{1,\frac{1}{2}}(X_T) \,\middle|\, (\partial_t - \nabla \cdot \gamma \nabla) u \in L^2(X_T) \right\},$$

where $\gamma = 1 + (k-1)\chi_D$, and χ_D is the characteristic function of D.

In this paper, we work in the above Sobolev spaces, and solutions to initial-boundary value problems should be understood in the weak sense. For example, the solution to (1.1) should be interpreted as follows. For given $g \in H^{-\frac{1}{2},-\frac{1}{4}}((\partial\Omega)_T)$, we seek $u \in \tilde{H}^{1,\frac{1}{2}}(\Omega_T;\, \partial_t - \nabla \cdot \gamma \nabla)$ such that

$$\int_0^T \int_\Omega \left(\gamma \nabla u \cdot \nabla v + \frac{\partial u}{\partial t} v \right) dx dt = \langle g,\, \Gamma v \rangle$$

for any $v \in \hat{H}^{1,\frac{1}{2}}(\Omega_T)$, where Γ is the Dirichlet trace map on $(\partial\Omega)_T$ and $\langle \cdot,\, \cdot \rangle$ should be understood in the sense of duality.

For later use, we denote by

$$G^a(x,\, t;\, y,\, s) := \begin{cases} \dfrac{1}{4a\pi\,(t-s)} \exp\left(-\dfrac{|x-y|^2}{4a(t-s)} \right), & t > s, \\ 0, & t \leq s \end{cases} \tag{2.1}$$

the fundamental solution of the heat operator $\partial_t - a\Delta$, where a is a constant. We sometimes write it as $G^a_{(y,\, s)}(x,\, t)$.

Note that $\Lambda_\emptyset$ is defined by $\Lambda_\emptyset g := v|_{(\partial\Omega)_T}$ with v satisfying

$$\begin{cases} (\partial_t - \Delta) v = 0 & \text{in } \Omega_T, \\ \partial_\nu v = g & \text{on } (\partial\Omega)_T, \\ v = 0 & \text{at } t = 0. \end{cases} \tag{2.2}$$

Define the operator

$$F := \Lambda_D - \Lambda_\emptyset.$$

Then our reconstruction scheme is based on the characterization of the solution to the Neumann-to-Dirichlet map gap equation

$$(Fg)(x,\, t) = G^\Omega_{(y,\, s)}(x,\, t), \quad (x,\, t) \in (\partial\Omega)_T \tag{2.3}$$

for a fixed time $s \in (0,\, T)$ and the sampling point $y \in \Omega$.

First, we analyze the solvability of (2.3).

Theorem 2.1. *For $y \in D$ and $s \in (0,\ T)$, the equation (2.3) has a solution if and only if the interior transmission problem*

$$\begin{cases} (\partial_t - \nabla \cdot k\nabla) w = 0 & \text{in } D_T, \\ (\partial_t - \Delta) v = 0 & \text{in } D_T, \\ w - v = G^{\Omega}_{(y,\,s)}(x,\,t) & \text{on } (\partial D)_T, \\ k\partial_\nu w - \partial_\nu v = \partial_\nu G^{\Omega}_{(y,\,s)}(x,\,t) & \text{on } (\partial D)_T, \\ w = 0 & \text{at } t = 0, \\ v = 0 & \text{at } t = 0 \end{cases} \tag{2.4}$$

is solvable with the solution w and v satisfying the equations $(\partial_t - \nabla \cdot \gamma\nabla) w = 0$ and $(\partial_t - \Delta) v = 0$ in Ω_T, respectively.

Proof. Suppose that $g \in H^{-\frac{1}{2},-\frac{1}{4}}((\partial\Omega)_T)$ is a solution to (2.3). Let w and v satisfy

$$\begin{cases} (\partial_t - \nabla \cdot \gamma\nabla) w = 0 & \text{in } \Omega_T, \\ \partial_\nu w = g & \text{on } (\partial\Omega)_T, \\ w = 0 & \text{at } t = 0 \end{cases} \tag{2.5}$$

and

$$\begin{cases} (\partial_t - \Delta) v = 0 & \text{in } \Omega_T, \\ \partial_\nu v = g & \text{on } (\partial\Omega)_T, \\ v = 0 & \text{at } t = 0, \end{cases} \tag{2.6}$$

respectively. Then we have

$$\begin{aligned} &w - v = \Lambda_D g - \Lambda_\emptyset g = G^{\Omega}_{(y,\,s)} \qquad \text{on } (\partial\Omega)_T, \\ &\partial_\nu w - \partial_\nu v = 0 = \partial_\nu G^{\Omega}_{(y,\,s)} \qquad \text{on } (\partial\Omega)_T, \end{aligned}$$

and therefore

$$w - v = G^{\Omega}_{(y,\,s)} \qquad \text{in } (\Omega \setminus \overline{D})_T.$$

By the continuities of w and v across ∂D, we further have

$$\begin{aligned} &w|_- - v|_- = G^{\Omega}_{(y,\,s)} \qquad \text{on } (\partial D)_T, \\ &k\partial_\nu w|_- - \partial_\nu v|_- = \partial_\nu G^{\Omega}_{(y,\,s)} \qquad \text{on } (\partial D)_T. \end{aligned}$$

Totally, we have the interior transmission problem (2.4).

Conversely, assume that $(w,\ v)$ is a solution to (2.4) and satisfies the equations $(\partial_t - \nabla \cdot \gamma\nabla) w = 0$ and $(\partial_t - \Delta) v = 0$ in Ω_T, respectively. By the continuities of w and v across ∂D, we obtain from the transmission conditions in (2.4) that

$$\begin{aligned} &w|_+ - v|_+ = G^{\Omega}_{(y,\,s)} \qquad \text{on } (\partial D)_T, \\ &\partial_\nu w|_+ - \partial_\nu v|_+ = \partial_\nu G^{\Omega}_{(y,\,s)} \qquad \text{on } (\partial D)_T. \end{aligned}$$

Notice that $w - v$ satisfies the heat equation $(\partial_t - \Delta)(w - v) = 0$ in $(\Omega \setminus \overline{D})_T$. Then it follows from the unique continuation principle that

$$w - v = G^{\Omega}_{(y,\,s)} \qquad \text{in } (\Omega \setminus \overline{D})_T, \tag{2.7}$$

and hence

$$w - v = G^{\Omega}_{(y,\,s)}, \quad \partial_\nu (w - v) = \partial_\nu G^{\Omega}_{(y,\,s)} \qquad \text{on } (\partial\Omega)_T. \tag{2.8}$$

This implies that $\partial_\nu w = \partial_\nu v$ on $(\partial\Omega)_T$ and $g := \partial_\nu v$ is the solution to (2.3). The proof is now complete. □

This theorem analyzes the solvability of the Neumann-to-Dirichlet map gap equation (2.3). Furthermore, if it does exist a solution, we explain what is the solution in the following theorem.

Theorem 2.2. *If g is the solution to (2.3), we let v be the solution to (2.6) with the boundary data $\partial_\nu v|_{(\partial\Omega)_T} = g$. Then we can conclude that*

$$v = G^D_{(y,s)}(x,t) - G^\Omega_{(y,s)}(x,t) \quad \text{in } D_T, \tag{2.9}$$

where $G^D_{(y,s)}(x,t)$ is defined by

$$\begin{cases} (\partial_t - \nabla\cdot k\nabla) H^D_{(y,s)} = 0 & \text{in } D_T, \\ (\partial_t - \Delta) G^D_{(y,s)} = \delta(x-y)\,\delta(t-s) & \text{in } D_T, \\ H^D_{(y,s)} - G^D_{(y,s)} = 0 & \text{on } (\partial D)_T, \\ k\partial_\nu H^D_{(y,s)} - \partial_\nu G^D_{(y,s)} = 0 & \text{on } (\partial D)_T, \\ H^D_{(y,s)} = 0 & \text{at } t = 0, \\ G^D_{(y,s)} = 0 & \text{at } t = 0. \end{cases} \tag{2.10}$$

Proof. Set

$$\tilde{G}^D_{(y,s)}(x,t) = G^D_{(y,s)}(x,t) - G^1_{(y,s)}(x,t), \tag{2.11}$$

$$\tilde{G}^\Omega_{(y,s)}(x,t) = G^\Omega_{(y,s)}(x,t) - G^1_{(y,s)}(x,t). \tag{2.12}$$

Note that $\tilde{G}^\Omega_{(y,s)}(x,t)$ is the reflected solution of the fundamental solution $G^1_{(y,s)}(x,t)$ in Ω_T and satisfies

$$\begin{cases} (\partial_t - \Delta)\tilde{G}^\Omega_{(y,s)} = 0 & \text{in } \Omega_T, \\ \partial_\nu \tilde{G}^\Omega_{(y,s)} = -\partial_\nu G^1_{(y,s)}(x,t) & \text{on } (\partial\Omega)_T, \\ \tilde{G}^\Omega_{(y,s)} = 0 & \text{at } t = 0. \end{cases}$$

We observe from (2.10) that

$$\begin{cases} (\partial_t - \nabla\cdot k\nabla) H^D_{(y,s)} = 0 & \text{in } D_T, \\ (\partial_t - \Delta)\tilde{G}^D_{(y,s)} = 0 & \text{in } D_T, \\ H^D_{(y,s)} - \tilde{G}^D_{(y,s)} = G^1_{(y,s)}(x,t) & \text{on } (\partial D)_T, \\ k\partial_\nu H^D_{(y,s)} - \partial_\nu \tilde{G}^D_{(y,s)} = \partial_\nu G^1_{(y,s)}(x,t) & \text{on } (\partial D)_T, \\ H^D_{(y,s)} = 0 & \text{at } t = 0, \\ \tilde{G}^D_{(y,s)} = 0 & \text{at } t = 0. \end{cases}$$

Let w and v be the solutions to (2.5) and (2.6) with the same boundary data $\partial_\nu v|_{(\partial\Omega)_T} = g$, respectively. Then we have

$$\begin{cases} (\partial_t - \nabla\cdot k\nabla)(w - H^D_{(y,s)}) = 0 & \text{in } D_T, \\ (\partial_t - \Delta)(v - \tilde{G}^D_{(y,s)} + \tilde{G}^\Omega_{(y,s)}) = 0 & \text{in } D_T, \\ (w - H^D_{(y,s)}) - (v - \tilde{G}^D_{(y,s)} + \tilde{G}^\Omega_{(y,s)}) = 0 & \text{on } (\partial D)_T, \\ k\partial_\nu(w - H^D_{(y,s)}) - \partial_\nu(v - \tilde{G}^D_{(y,s)} + \tilde{G}^\Omega_{(y,s)}) = 0 & \text{on } (\partial D)_T, \\ w - H^D_{(y,s)} = 0 & \text{at } t = 0, \\ v - \tilde{G}^D_{(y,s)} + \tilde{G}^\Omega_{(y,s)} = 0 & \text{at } t = 0. \end{cases} \tag{2.13}$$

The uniqueness of solutions to the interior transmission problem (2.4) says that

$$v = \tilde{G}^D_{(y,s)}(x,t) - \tilde{G}^\Omega_{(y,s)}(x,t) \quad \text{in } D_T,$$

which gives (2.9) and completes the proof. □

Here we would like to emphasize that the reflected solution $\tilde{G}^\Omega_{(y,s)}(x,t)$ and the Green function $G^\Omega_{(y,s)}(x,t)$ are completely determined by the domain Ω. So they are actually known in our inverse problem. Thus, once we have the solution

g to (2.3), we solve the initial-boundary value problem (2.6) with the boundary data $\partial_\nu v = g$ on $(\partial\Omega)_T$ and then obtain the Green function $G^D_{(y,s)}(x,t) = v + G^\Omega_{(y,s)}(x,t)$. In this sense, our reconstruction method in principle provides a way of computing the Green function $G^D_{(y,s)}(x,t)$ for the interior transmission problem (2.4) from the Neumann-to-Dirichlet map Λ_D.

For $y \in \Omega \setminus \overline{D}$, we have proven the following result in our previous work [17]:

Theorem 2.3. *For $s \in (0, T)$ and $y \in \Omega \setminus \overline{D}$, the equation (2.3) has no solution.*

According to Theorems 2.2 and 2.3, we cannot guarantee the solvability of (2.3). However, we could find an approximation solution in some sense that characterizes the boundary of the inclusion. The theoretical results are obtained in [17] and can be summarized as follows.

Theorem 2.4. *Let $s \in (0, T)$ be fixed. We have the following conclusions:*

(1) *if $y \in D$, then for any $\varepsilon > 0$ there exists a function $g^y \in H^{-\frac{1}{2},-\frac{1}{4}}((\partial\Omega)_T)$ satisfying*

$$\|Fg^y - G^\Omega_{(y,s)}\|_{H^{\frac{1}{2},\frac{1}{4}}((\partial\Omega)_T)} < \varepsilon$$

such that

$$\lim_{y\to\partial D} \|g^y\|_{H^{-\frac{1}{2},-\frac{1}{4}}((\partial\Omega)_T)} = \infty \tag{2.14}$$

and

$$\lim_{y\to\partial D} \|Sg^y\|_{\tilde{H}^{1,\frac{1}{2}}(D_T)} = \infty, \tag{2.15}$$

where the operator S is defined by

$$S : H^{-\frac{1}{2},-\frac{1}{4}}((\partial\Omega)_T) \to \tilde{H}^{1,\frac{1}{2}}(D_T), \quad g^y \mapsto v|_{D_T},$$

with v being the solution to (2.2);

(2) *if $y \in \Omega \setminus \overline{D}$, then for any $\varepsilon,\ \eta > 0$ there exists a function $g^y \in H^{-\frac{1}{2},-\frac{1}{4}}((\partial\Omega)_T)$ satisfying*

$$\|Fg^y - G^\Omega_{(y,s)}\|_{H^{\frac{1}{2},\frac{1}{4}}((\partial\Omega)_T)} < \varepsilon + \eta$$

such that

$$\lim_{\eta\to 0} \|g^y\|_{H^{-\frac{1}{2},-\frac{1}{4}}((\partial\Omega)_T)} = \infty \tag{2.16}$$

and

$$\lim_{\eta\to 0} \|Sg^y\|_{\tilde{H}^{1,\frac{1}{2}}(D_T)} = \infty. \tag{2.17}$$

Based on Theorem 2.4, we define the indicator function by

$$I(y) := \|g^y\|_{H^{-\frac{1}{2},-\frac{1}{4}}((\partial\Omega)_T)}$$

and reconstruct the geometric information on D using the following algorithm:

Algorithm 2.5.

1. Fix $s \in (0, T)$ and select a set of "sampling points y" in Ω;
2. Compute an approximate solution to the equation (2.3) for each sampling point;
3. Assert that $y \in D$ if and only if $I(y) \le C$, where the cut-off constant C should be chosen properly.

In practice, the measurement data always contain some noise, so the operator F cannot be given exactly and some regularization technique is necessary in numerical implementations. Denote by F^δ the perturbed operator of F with

$$\|F^\delta - F\| \le \delta,$$

where δ is the noise level and $\|\cdot\|$ is the operator norm. Using the Tikhonov regularization method, we construct an approximate solution to the perturbed Neumann-to-Dirichlet map gap equation

$$F^\delta g = G^\Omega_{(y,s)}$$

by

$$g^y_{\alpha,\delta} := \left[\alpha I + (F^\delta)^* F^\delta\right]^{-1} \left(F^\delta\right)^* \left[G^\Omega_{(y,s)}\right]. \tag{2.18}$$

Then we have the following convergence result:

Theorem 2.6. *Let $y \in D$ and the Neumann-to-Dirichlet map gap equation (2.3) have a unique solution g^y. If we choose the regularization parameter α properly such that $\alpha(\delta) \to 0$ and $\frac{\delta}{\alpha^{3/2}(\delta)} \to 0$ as $\delta \to 0$, then it holds that*

$$g^y_{\alpha,\delta} \to g^y \qquad \text{as } \delta \to 0. \tag{2.19}$$

Proof. By direct calculations, we have

$$\begin{aligned} g^y_{\alpha,\delta} - g^y = &\left\{\left[\alpha I + \left(F^\delta\right)^* F^\delta\right]^{-1} - \left[\alpha I + F^*F\right]^{-1}\right\} \left(F^\delta\right)^* \left[G^\Omega_{(y,s)}\right] \\ &+ \left[\alpha I + F^*F\right]^{-1} \left[\left(F^\delta\right)^* - F^*\right] \left[G^\Omega_{(y,s)}\right] \\ &+ \left[\alpha I + F^*F\right]^{-1} F^* \left[G^\Omega_{(y,s)}\right] - g^y. \end{aligned} \tag{2.20}$$

From the estimate

$$\left\|\left[\alpha I + \left(F^\delta\right)^* F^\delta\right]^{-1} - \left[\alpha I + F^*F\right]^{-1}\right\| \le \frac{2\delta}{\alpha^{3/2}},$$

we have

$$\left\{\left[\alpha I + \left(F^\delta\right)^* F^\delta\right]^{-1} - \left[\alpha I + F^*F\right]^{-1}\right\} \left(F^\delta\right)^* \left[G^\Omega_{(y,s)}\right] \le \left\|\left(F^\delta\right)^*\right\| \left\|G^\Omega_{(y,s)}\right\| \frac{2\delta}{\alpha^{3/2}}. \tag{2.21}$$

Notice that

$$\|(\alpha I + B)^{-1}\| \le \frac{1}{\alpha}$$

holds for any self-adjoint and positive operator B in Hilbert space. Then we obtain that

$$\left\|\left[\alpha I + F^*F\right]^{-1} \left[\left(F^\delta\right)^* - F^*\right] \left[G^\Omega_{(y,s)}\right]\right\| \le \left\|G^\Omega_{(y,s)}\right\| \frac{\delta}{\alpha}. \tag{2.22}$$

In addition, it follows from standard regularization theory that

$$\left[\alpha I + F^*F\right]^{-1} F^* \left[G^\Omega_{(y,s)}\right] \to g^y \qquad \text{as } \alpha \to 0.$$

Thus, the proof is completed by combining it with the estimates (2.21) and (2.22). □

Remark 2.7. By the well-posedness of the initial-boundary value problem (2.2) and the equality (2.9), we can easily deduce from (2.19) that

$$\left\|S[g^y_{\alpha,\delta}] - \left(G^D_{(y,s)}(x,t) - G^\Omega_{(y,s)}(x,t)\right)\right\|_{\tilde{H}^{1,\frac{1}{2}}(D_T)} \to 0 \quad \text{as } \delta \to 0, \tag{2.23}$$

which leads to the convergence for computing the Green function $G^D_{(y,s)}(x,t)$ from the Neumann-to-Dirichlet map Λ_D.

3. Numerical scheme for solving the direct problem

In this section, we present a numerical scheme to solve the forward problem (1.1) for two-dimensional spatial domains. Based on the potential theory for the heat equation, we first reformulate the initial-boundary value problem (1.1) as a system of boundary integral equations, and then introduce a discretization scheme for solving this system. This scheme is an extension of the method proposed in [2,3] to the layered medium case. Our problem (1.1) involves the operator $\partial_t - a\Delta$ with $a = 1, k$, so the discretization of the integral operators for a general constant a will be considered.

Define the following heat layer potentials:

$$V_{ij}^a[\varphi](x,\,t) := \int_0^t \int_{S_i} G^a(x,\,t;\,y,\,s)\varphi(y,\,s)\,d\sigma(y)ds, \quad (x,\,t) \in S_j \times (0,\,T),$$

$$N_{ij}^a[\varphi](x,\,t) := \int_0^t \int_{S_i} \frac{\partial G^a(x,\,t;\,y,\,s)}{\partial \nu(x)}\varphi(y,\,s)\,d\sigma(y)ds, \quad (x,\,t) \in S_j \times (0,\,T),$$

where $G^a(x,\,t;\,y,\,s)$ is the fundamental solution defined by (2.1). Later we will take $i,\,j = 1,\,2$ with $S_1 = \partial D$ and $S_2 = \partial\Omega$.

Assume that D is a homogeneous inclusion, that is, k is a constant. We express the solution u to (1.1) by the following single-layer potentials:

$$u(x,\,t) = \int_0^t \int_{\partial D} G^k(x,\,t;\,y,\,s)\varphi_1(y,\,s)\,d\sigma(y)ds, \qquad (x,\,t) \in D_T, \tag{3.1}$$

$$\begin{aligned} u(x,\,t) = &\int_0^t \int_{\partial D} G^1(x,\,t;\,y,\,s)\varphi_2(y,\,s)\,d\sigma(y)ds \\ &+ \int_0^t \int_{\partial\Omega} G^1(x,\,t;\,y,\,s)\varphi_3(y,\,s)\,d\sigma(y)ds, \qquad (x,\,t) \in (\Omega \setminus \overline{D})_T, \end{aligned} \tag{3.2}$$

where φ_1, φ_2 and φ_3 are density functions to be determined. Using jump relations of heat layer potentials [4], we can verify that u expressed by (3.1) and (3.2) is the solution to (1.1) provide that φ_1, φ_2 and φ_3 satisfy

$$V_{11}^k[\varphi_1] - V_{11}^1[\varphi_2] - V_{21}^1[\varphi_3] = 0, \tag{3.3}$$

$$\varphi_1 + 2kN_{11}^k[\varphi_1] + \varphi_2 - 2N_{11}^1[\varphi_2] - 2N_{21}^1[\varphi_3] = 0, \tag{3.4}$$

$$2N_{12}^1[\varphi_2] + \varphi_3 + 2N_{22}^1[\varphi_3] = 2g. \tag{3.5}$$

Note that the integral kernels of V_{21}^1, N_{21}^1 and N_{12}^1 are smooth, while those of V_{11}^k, N_{11}^k, V_{11}^1, N_{11}^1 and N_{22}^1 are singular at $(x,\,t) = (y,\,s)$. To numerically solve the equations (3.3)-(3.5), we present a discretization scheme as follows [2,3].

Assume that the boundaries ∂D and $\partial\Omega$ have the parametric representations

$$\partial D = \{x_1(\alpha) : x_1(\alpha) = (x_{11}(\alpha),\,x_{12}(\alpha)),\ 0 \le \alpha \le 2\pi\},$$

$$\partial\Omega = \{x_2(\alpha) : x_2(\alpha) = (x_{21}(\alpha),\,x_{22}(\alpha)),\ 0 \le \alpha \le 2\pi\},$$

where $x_{ij}(x)$ $(i,\,j = 1,\,2)$ are of class C^2 and 2π-periodic functions. The unit outward normal vectors on ∂D and $\partial\Omega$ are given by

$$\nu_1(\alpha) = \frac{(x_{12}'(\alpha),\,-x_{11}'(\alpha))}{|x_1'(\alpha)|}, \qquad \nu_2(\alpha) = \frac{(x_{22}'(\alpha),\,-x_{21}'(\alpha))}{|x_2'(\alpha)|}.$$

Set $\tilde{\varphi}_1(\beta,\,s) := \varphi_1(x_1(\beta),\,s)$, $\tilde{\varphi}_2(\beta,\,s) := \varphi_2(x_1(\beta),\,s)$, $\tilde{\varphi}_3(\beta,\,s) := \varphi_3(x_2(\beta),\,s)$, $r_{ij}(\alpha,\,\beta) = |x_j(\alpha) - x_i(\beta)|$.

We apply a collocation method using piecewise constant interpolation with respect to the time variable on the equidistant grid $t_n := nT/N$, $n = 0,\,1,\,\cdots,\,N$. That is, we approximate the density $\tilde{\varphi}_i(\beta,\,s)$ by

$$\tilde{\varphi}_i(\beta,\,s) \approx \sum_{n=1}^{N} \tilde{\varphi}_{i,n}(\beta)\Phi_n(s),$$

where $\tilde{\varphi}_{i,n}(\beta) := \tilde{\varphi}_i(\beta,\,t_n)$, $i = 1,\,2,\,3$ and

$$\Phi_n(s) := \begin{cases} 1, & t_{n-1} < s \le t_n, \\ 0, & \text{otherwise.} \end{cases}$$

Take

$$K_{ij}^{a,\,p}(\alpha,\,\beta) := \begin{cases} \frac{1}{4\pi a}E_1\left(\frac{Nr_{ij}^2(\alpha,\,\beta)}{4aT}\right), & p = 0, \\ \frac{1}{4\pi a}E_1\left(\frac{Nr_{ij}^2(\alpha,\,\beta)}{4aT(p+1)}\right) - \frac{1}{4\pi a}E_1\left(\frac{Nr_{ij}^2(\alpha,\,\beta)}{4aTp}\right), & p = 1,\,\cdots,\,N-1, \end{cases} \tag{3.6}$$

where E_1 is the exponential integral function defined by

$$E_1(z) = \int_1^{+\infty} \frac{e^{-tz}}{t} dt = \int_0^1 \frac{e^{-z/u}}{u} du.$$

Note that $K_{jj}^{a,0}$ has logarithmic singularity and can be decomposed into

$$K_{jj}^{a,0}(\alpha, \beta) = -\frac{1}{4\pi a} \ln\left(\frac{4}{e} \sin^2 \frac{\alpha-\beta}{2}\right) + \tilde{K}_{jj}^{a,0}(\alpha, \beta), \quad \alpha \neq \beta,$$

where

$$\tilde{K}_{jj}^{a,0}(\alpha, \beta) = K_{jj}^{a,0}(\alpha, \beta) + \frac{1}{4\pi a} \ln\left(\frac{4}{e} \sin^2 \frac{\alpha-\beta}{2}\right), \quad \alpha \neq \beta$$

with

$$\lim_{\beta\to\alpha} \tilde{K}_{jj}^{a,0}(\alpha, \beta) = -\frac{\gamma_E}{4\pi a} - \frac{1}{4\pi a} \ln\left(\frac{eN|x_j'(\alpha)|^2}{4aT}\right).$$

Here $\gamma_E = 0.55721$ is the Euler constant. It is easy to see that

$$\lim_{\beta\to\alpha} K_{jj}^{a,p}(\alpha, \beta) = \frac{1}{4\pi a} \ln\frac{p+1}{p}, \quad p = 1, \cdots, N-1.$$

For $i \neq j$ the kernels $K_{ij}^{a,p}$ are continuous for $p = 0, 1, \cdots, N-1$.

Set

$$L_{ij}^{a,p}(\alpha, \beta) := \begin{cases} \frac{(x_i(\beta)-x_j(\alpha))\cdot\nu_j(\alpha)|x_i'(\beta)|}{2\pi a r_{ij}^2(\alpha,\beta)} \exp\left(-\frac{Nr_{ij}^2(\alpha,\beta)}{4aT}\right), & p = 0, \\ \frac{(x_i(\beta)-x_j(\alpha))\cdot\nu_j(\alpha)|x_i'(\beta)|}{2\pi a r_{ij}^2(\alpha,\beta)} \left\{\exp\left(-\frac{Nr_{ij}^2(\alpha,\beta)}{4aT(p+1)}\right) - \exp\left(-\frac{Nr_{ij}^2(\alpha,\beta)}{4aTp}\right)\right\}, & p = 1, \cdots, N-1. \end{cases}$$

For $i = j$, we can easily deduce that

$$\lim_{\beta\to\alpha} L_{jj}^{a,0}(\alpha, \beta) = \frac{x_{j1}''(\alpha)x_{j2}'(\alpha) - x_{j1}'(\alpha)x_{j2}''(\alpha)}{4\pi a|x_j'(\alpha)|^2}, \tag{3.7}$$

$$\lim_{\beta\to\alpha} L_{jj}^{a,p}(\alpha, \beta) = 0, \quad p = 1, \cdots, N-1. \tag{3.8}$$

For $i \neq j$, the kernels $L_{ij}^{a,p}$ are continuous for $p = 0, 1, \cdots, N-1$.

Then, by the same derivations as in [2,3], we have

$$V_{ij}^a[\varphi_i](x_j(\alpha), t_n) \approx \sum_{m=1}^{n} \int_0^{2\pi} K_{ij}^{a,n-m}(\alpha, \beta)\tilde{\varphi}_{i,m}(\beta)|x_i'(\beta)| d\beta,$$

$$N_{ij}^a[\varphi_i](x_j(\alpha), t_n) \approx \sum_{m=1}^{n} \int_0^{2\pi} L_{ij}^{a,n-m}(\alpha, \beta)\tilde{\varphi}_{i,m}(\beta) d\beta.$$

Using these approximations and setting $t = t_n$ for (3.3)–(3.5), we have the following integral equations:

$$\begin{aligned} &\int_0^{2\pi} K_{11}^{k,0}(\alpha, \beta)|x_1'(\beta)|\tilde{\varphi}_{1,n}(\beta) d\beta - \int_0^{2\pi} K_{11}^{1,0}(\alpha, \beta)|x_1'(\beta)|\tilde{\varphi}_{2,n}(\beta) d\beta - \int_0^{2\pi} K_{21}^{1,0}(\alpha, \beta)|x_2'(\beta)|\tilde{\varphi}_{3,n}(\beta) d\beta \\ &= -\sum_{m=1}^{n-1} \int_0^{2\pi} K_{11}^{k,n-m}(\alpha, \beta)|x_1'(\beta)|\tilde{\varphi}_{1,m}(\beta) d\beta + \sum_{m=1}^{n-1} \int_0^{2\pi} K_{11}^{1,n-m}(\alpha, \beta)|x_1'(\beta)|\tilde{\varphi}_{2,m}(\beta) d\beta \\ &\quad + \sum_{m=1}^{n-1} \int_0^{2\pi} K_{21}^{1,n-m}(\alpha, \beta)|x_2'(\beta)|\tilde{\varphi}_{3,m}(\beta) d\beta, \end{aligned} \tag{3.9}$$

$$\frac{1}{2}\tilde{\varphi}_{1,n}(\alpha)+k\int_0^{2\pi}L_{11}^{k,0}(\alpha,\,\beta)\tilde{\varphi}_{1,n}(\beta)\,d\beta+\frac{1}{2}\tilde{\varphi}_{2,n}(\alpha)-\int_0^{2\pi}L_{11}^{1,0}(\alpha,\,\beta)\tilde{\varphi}_{2,n}(\beta)\,d\beta-\int_0^{2\pi}L_{21}^{1,0}(\alpha,\,\beta)\tilde{\varphi}_{3,n}(\beta)\,d\beta$$

$$=-k\sum_{m=1}^{n-1}\int_0^{2\pi}L_{11}^{k,n-m}(\alpha,\,\beta)\tilde{\varphi}_{1,m}(\beta)\,d\beta+\sum_{m=1}^{n-1}\int_0^{2\pi}L_{11}^{1,n-m}(\alpha,\,\beta)\tilde{\varphi}_{2,m}(\beta)\,d\beta+\sum_{m=1}^{n-1}\int_0^{2\pi}L_{21}^{1,n-m}(\alpha,\,\beta)\tilde{\varphi}_{3,m}(\beta)\,d\beta, \tag{3.10}$$

$$\int_0^{2\pi}L_{12}^{1,0}(\alpha,\,\beta)\tilde{\varphi}_{2,n}(\beta)\,d\beta+\frac{1}{2}\tilde{\varphi}_{3,n}(\alpha)+\int_0^{2\pi}L_{22}^{1,0}(\alpha,\,\beta)\tilde{\varphi}_{3,n}(\beta)\,d\beta$$

$$=\tilde{g}(\alpha,\,t_n)-\sum_{m=1}^{n-1}\int_0^{2\pi}L_{12}^{1,n-m}(\alpha,\,\beta)\tilde{\varphi}_{2,m}(\beta)\,d\beta-\sum_{m=1}^{n-1}\int_0^{2\pi}L_{22}^{1,n-m}(\alpha,\,\beta)\tilde{\varphi}_{3,m}(\beta)\,d\beta, \tag{3.11}$$

where $\tilde{g}(\alpha,\,t_n)=g(x_2(\alpha),\,t_n)$.

For the discretization with respect to the space variable, we apply the Nyström method to the above integral equations using the trapezoidal rule on the equidistant mesh $\beta_j:=j\pi/M,\ j=0,\cdots,2M-1$. Especially, for the integral involving $K_{11}^{a,0}(\alpha,\,\beta)$, we need to deal with the singular integral of the form

$$\int_0^{2\pi}\ln\left(\frac{4}{e}\sin^2\frac{\alpha-\beta}{2}\right)\varphi(\beta)\,d\beta.$$

In fact, it can be computed approximately by the quadrature rule

$$\int_0^{2\pi}\ln\left(\frac{4}{e}\sin^2\frac{\alpha_i-\beta}{2}\right)\varphi(\beta)\,d\beta\approx 2\pi\sum_{j=0}^{2M-1}R_{|i-j|}\varphi(\alpha_j) \tag{3.12}$$

for $\alpha_j:=j\pi/M,\ j=0,\cdots,2M-1$, where the weights are given by

$$R_j:=-\frac{1}{2M}\left\{1+2\sum_{m=1}^{M-1}\frac{1}{m}\cos(m\alpha_j)+\frac{(-1)^j}{M}\right\},\quad j=0,\,1,\cdots,2M-1.$$

Finally, we have the following linear system:

$$\begin{aligned}
&-\frac{1}{2k}\sum_{j=0}^{2M-1}R_{|i-j|}|x_1'(\beta_j)|\tilde{\varphi}_{1,n;\,j}+\frac{\pi}{M}\sum_{j=0}^{2M-1}\tilde{K}_{11}^{k,0}(\beta_i,\,\beta_j)|x_1'(\beta_j)|\tilde{\varphi}_{1,n;\,j}\\
&+\frac{1}{2}\sum_{j=0}^{2M-1}R_{|i-j|}|x_1'(\beta_j)|\tilde{\varphi}_{2,n;\,j}-\frac{\pi}{M}\sum_{j=0}^{2M-1}\tilde{K}_{11}^{1,0}(\beta_i,\,\beta_j)|x_1'(\beta_j)|\tilde{\varphi}_{2,n;\,j}\\
&-\frac{\pi}{M}\sum_{j=0}^{2M-1}K_{21}^{1,0}(\beta_i,\,\beta_j)|x_2'(\beta_j)|\tilde{\varphi}_{3,n;\,j}\\
&=-\frac{\pi}{M}\sum_{j=0}^{2M-1}\sum_{m=1}^{n-1}K_{11}^{k,n-m}(\beta_i,\,\beta_j)|x_1'(\beta_j)|\tilde{\varphi}_{1,m;\,j}+\frac{\pi}{M}\sum_{j=0}^{2M-1}\sum_{m=1}^{n-1}K_{11}^{1,n-m}(\beta_i,\,\beta_j)|x_1'(\beta_j)|\tilde{\varphi}_{2,m;\,j}\\
&+\frac{\pi}{M}\sum_{j=0}^{2M-1}\sum_{m=1}^{n-1}K_{21}^{1,n-m}(\beta_i,\,\beta_j)|x_2'(\beta_j)|\tilde{\varphi}_{3,m;\,j},
\end{aligned} \tag{3.13}$$

$$\begin{aligned}
&\frac{1}{2}\tilde{\varphi}_{1,n;i}+k\frac{\pi}{M}\sum_{j=0}^{2M-1}L_{11}^{k,0}(\beta_i,\,\beta_j)\tilde{\varphi}_{1,n;\,j}+\frac{1}{2}\tilde{\varphi}_{2,n;i}-\frac{\pi}{M}\sum_{j=0}^{2M-1}L_{11}^{1,0}(\beta_i,\,\beta_j)\tilde{\varphi}_{2,n;\,j}-\frac{\pi}{M}\sum_{j=0}^{2M-1}L_{21}^{1,0}(\beta_i,\,\beta_j)\tilde{\varphi}_{3,n;\,j}\\
&=-k\frac{\pi}{M}\sum_{m=1}^{n-1}L_{11}^{k,n-m}(\beta_i,\,\beta_j)\tilde{\varphi}_{1,m;\,j}+\frac{\pi}{M}\sum_{m=1}^{n-1}L_{11}^{1,n-m}(\beta_i,\,\beta_j)\tilde{\varphi}_{2,m;\,j}+\frac{\pi}{M}\sum_{m=1}^{n-1}L_{21}^{1,n-m}(\beta_i,\,\beta_j)\tilde{\varphi}_{3,m;\,j},
\end{aligned} \tag{3.14}$$

$$\frac{\pi}{M}\sum_{j=0}^{2M-1} L_{12}^{1,0}(\beta_i,\,\beta_j)\tilde{\varphi}_{2,n;\,j}+\frac{1}{2}\tilde{\varphi}_{3,n;i}+\frac{\pi}{M}\sum_{j=0}^{2M-1} L_{22}^{1,0}(\beta_i,\,\beta_j)\tilde{\varphi}_{3,n;\,j}$$

$$=\tilde{g}(\alpha_i,\,t_n)-\frac{\pi}{M}\sum_{m=1}^{n-1} L_{12}^{1,n-m}(\beta_i,\,\beta_j)\tilde{\varphi}_{2,m;\,j}-\frac{\pi}{M}\sum_{m=1}^{n-1} L_{22}^{1,n-m}(\beta_i,\,\beta_j)\tilde{\varphi}_{3,m;\,j}, \tag{3.15}$$

for $\tilde{\varphi}_{1,n;i}:=\tilde{\varphi}_{1,n}(\beta_i)$, $\tilde{\varphi}_{2,n;i}:=\tilde{\varphi}_{2,n}(\beta_i)$, $\tilde{\varphi}_{3,n;i}:=\tilde{\varphi}_{3,n}(\beta_i)$, $i=0,\cdots,2M-1$, $n=1,\cdots,N$. This system should be solved recursively for $n=1,\cdots,N$. For each n, we need to solve a system consisting of $6M$ linear equations with $6M$ unknowns. Its coefficient matrix $\mathbb{B}$ can be written as a block matrix in the following form:

$$\mathbb{B}=\begin{pmatrix} B^{11} & B^{12} & B^{13}\\ \frac{1}{2}I+B^{21} & \frac{1}{2}I+B^{22} & B^{23}\\ B^{31} & B^{32} & \frac{1}{2}I+B^{33}\end{pmatrix}=\begin{pmatrix} B^{11} & 0 & 0\\ \frac{1}{2}I & \frac{1}{2}I & 0\\ 0 & 0 & \frac{1}{2}I\end{pmatrix}+\begin{pmatrix} 0 & B^{12} & B^{13}\\ B^{21} & B^{22} & B^{23}\\ B^{31} & B^{32} & B^{33}\end{pmatrix}=:\mathbb{B}_1+\mathbb{B}_2$$

where B^{lk} $(l,k=1,2,3)$ are $2M\times 2M$ matrices with the matrix elements $B_{ij}^{11}=-\frac{1}{2k}R_{|i-j|}|x_1'(\beta_j)|+\frac{\pi}{M}\tilde{K}_{11}^{k,0}(\beta_i,\,\beta_j)|x_1'(\beta_j)|$, $B_{ij}^{12}=\frac{1}{2}R_{|i-j|}|x_1'(\beta_j)|-\frac{\pi}{M}\tilde{K}_{11}^{1,0}(\beta_i,\,\beta_j)|x_1'(\beta_j)|$, $B_{ij}^{13}=-\frac{\pi}{M}K_{21}^{1,0}(\beta_i,\,\beta_j)|x_2'(\beta_j)|$, $B_{ij}^{21}=k\frac{\pi}{M}L_{11}^{k,0}(\beta_i,\,\beta_j)$, $B_{ij}^{22}=-\frac{\pi}{M}L_{11}^{1,0}(\beta_i,\,\beta_j)$, $B_{ij}^{23}=-\frac{\pi}{M}L_{21}^{1,0}(\beta_i,\,\beta_j)$, $B_{ij}^{31}=0$, $B_{ij}^{32}=\frac{\pi}{M}L_{12}^{1,0}(\beta_i,\,\beta_j)$, $B_{ij}^{33}=\frac{\pi}{M}L_{22}^{1,0}(\beta_i,\,\beta_j)$. Then we can easily see that the above system is uniquely solvable, if B^{11} is invertible and -1 is not an eigenvalue of $\mathbb{B}_1^{-1}\mathbb{B}_2$.

Once we have obtained the density functions φ_1, φ_2 and φ_3 approximately by solving the above linear system, we compute $u(x,\,t)|_{(\partial\Omega)_T}$ in terms of (3.2):

$$\begin{aligned} u(x_2(\beta_i),\,t_n)\approx{}&\frac{\pi}{M}\sum_{m=1}^{n}\sum_{j=0}^{2M-1} K_{12}^{1,n-m}(\beta_i,\,\beta_j)|x_1'(\beta_j)|\tilde{\varphi}_{2,m;\,j}-\frac{1}{2}\sum_{j=0}^{2M-1} R_{|i-j|}|x_2'(\beta_j)|\tilde{\varphi}_{3,n;\,j}\\ &+\frac{\pi}{M}\sum_{j=0}^{2M-1}\tilde{K}_{22}^{1,0}(\beta_i,\,\beta_j)|x_2'(\beta_j)|\tilde{\varphi}_{3,n;\,j}\\ &+\frac{\pi}{M}\sum_{m=1}^{n-1}\sum_{j=0}^{2M-1} K_{22}^{1,n-m}(\beta_i,\,\beta_j)|x_2'(\beta_j)|\tilde{\varphi}_{3,m;\,j}\end{aligned} \tag{3.16}$$

for $i=0,\,1,\cdots,2M-1$, $n=1,\,2,\cdots,N$.

Based on the above discretization scheme, we can get the discretized version $\mathbb{A}_D$ of the Neumann-to-Dirichlet map Λ_D. Indeed, let

$$\mathbb{U}=(u(x_2(\beta_0),\,t_1),\cdots,u(x_2(\beta_{2M-1}),\,t_1),\cdots,u(x_2(\beta_0),\,t_N),\cdots,u(x_2(\beta_{2M-1}),\,t_N))^T,$$

$$\beta=(g(x_2(\beta_0),\,t_1),\cdots,g(x_2(\beta_{2M-1}),\,t_1),\cdots,g(x_2(\beta_0),\,t_N),\cdots,g(x_2(\beta_{2M-1}),\,t_N))^T.$$

Then, combining (3.13)–(3.15) and (3.16), we can assemble a matrix $\mathbb{A}_D\in\mathbb{R}^{2MN\times 2MN}$ such that

$$\mathbb{U}=\mathbb{A}_D\,\beta. \tag{3.17}$$

This implies that $\mathbb{A}_D$ is the discretized version of Λ_D. In the same way, we can obtain the discretized version $\mathbb{A}_\emptyset$ of $\Lambda_\emptyset$ by solving the initial-boundary value problem (2.2). So the operator F is discretized as the matrix $\mathbb{F}:=\mathbb{A}_D-\mathbb{A}_\emptyset$. Note that the Green function $G_{(y,\,s)}^{\Omega}(x,\,t)=G_{(y,\,s)}^{1}(x,\,t)+\tilde{G}_{(y,\,s)}^{\Omega}(x,\,t)$, where $\tilde{G}_{(y,\,s)}^{\Omega}(x,\,t)$ satisfies (2.2) with $g=-\partial_{\nu(x)}G_{(y,\,s)}^{1}(x,\,t)$. The function $\tilde{G}_{(y,\,s)}^{\Omega}(x,\,t)$ can also be computed by the above numerical method and the Green function $G_{(y,\,s)}^{\Omega}(x,\,t)$ are therefore obtained. Let

$$\mathbb{G}_{(y,\,s)}=\left(G_{(y,\,s)}^{\Omega}(x_2(\beta_0),\,t_1),\cdots,G_{(y,\,s)}^{\Omega}(x_2(\beta_{2M-1}),\,t_1),\cdots,G_{(y,\,s)}^{\Omega}(x_2(\beta_0),\,t_N),\cdots,G_{(y,\,s)}^{\Omega}(x_2(\beta_{2M-1}),\,t_N)\right)^T.$$

Then we are led to the following linear equation:

$$\mathbb{F}\,\beta=\mathbb{G}_{(y,\,s)}, \tag{3.18}$$

which is the discretized version of the Neumann-to-Dirichlet map gap equation (2.3).

4. Numerical examples

In this section, we present some numerical results to show the performance of the reconstruction method for our inverse problem. First, we simulate the operator $F = \Lambda_D - \Lambda_\emptyset$ and compute the Green function $G^{\Omega}_{(y,\,s)}(x,\,t)$ by the numerical scheme provided in Section 3. Then, taking the synthetic data as measurements, we solve the discretized Neumann-to-Dirichlet map gap equation (3.18) by the classical Tikhonov regularization method. In the first example, we implement the reconstruction method for one inclusion of three different shapes. The cases of different thermal conductivities, namely, $k < 1$ and $k > 1$, are tested. The second example is devoted to the numerical reconstruction by using short time measurements, where the measured data are only available in a very short time interval.

In all numerical experiments, we take $N = 100$, $M = 16$. This yields a 3200×3200 matrix $\mathbb{F} := (f_{ij})$ which is the discretized version of the operator $F = \Lambda_D - \Lambda_\emptyset$. The uniform random noise is added to $\mathbb{F}$ via

$$f^{\delta}_{ij} = f_{ij} \times (1 + \delta\, rd_{ij}),$$

where δ is the noise level and (rd_{ij}) is a matrix whose elements are normally distributed with mean value 0 and standard deviation 1. In all numerics, we take Ω as a circle with radius r and center at the origin. We choose 20×32 sampling points in Ω specified by

$$y_{ij} = r_i \left(\cos(\alpha_j),\, \sin(\alpha_j)\right), \quad r_i = \frac{r}{20} i,\, \alpha_j = \frac{\pi}{16} j, \quad i = 1, \cdots, 20,\; j = 1, \cdots, 32. \tag{4.1}$$

For each sampling point y_{ij}, we compute the indicator function $I(y_{ij})$ defined by

$$I(y_{ij}) := 1/\ln(\|g^{y_{ij}}\|_{L^2}). \tag{4.2}$$

Here we would like to mention that, instead of the norm of $g^{y_{ij}}$, we use (4.2) as the indicator function in our numerical experiments and it turns out to be more efficient.

Example 4.1. We test the reconstruction method for one inclusion of differential shapes. Let Ω be a circle with radius 3 centered at the origin. For the inclusion D, we consider the following three different shapes, namely, kite-shaped, boat-shaped and pear-shaped domains parameterized by

"Kite": $\partial D = \{(\cos(\alpha) + 0.65\cos(2\alpha) - 0.65,\, 1.5\sin(\alpha)) : \alpha \in [0,\, 2\pi]\}$;

"Boat": $\partial D = \{(0.5\cos(\alpha) - 0.1\sin(4\alpha),\, -1.5\sin(\alpha)) : \alpha \in [0,\, 2\pi]\}$;

"Pear": $\partial D = \{(1 + 0.3\cos(3\alpha))(\cos(\alpha), \sin(\alpha)) : \alpha \in [0,\, 2\pi]\}$.

Set $T = 1$ and $\delta = 0.05$.

The numerical reconstructions are shown in Figs. 4.1–4.3, where the left pictures show 100 contour lines of the indicator functions for $k = 0.5$ and the right pictures show those for $k = 2$. We can easily observe that the L^2-norm of g^y becomes significantly large as the sampling point y approaches the boundary ∂D and keeps large outside D. The numerical results greatly illustrate our theoretical analysis. We conclude that the reconstruction method works well for inclusions of differential shapes and thermal conductivities, and it has a high tolerance for the measurement noise.

Example 4.2. We test the reconstruction method with short time measurement. The domain Ω is taken as the same in Example 4.1. The inclusion D is set to be a boat or a pear defined above. Suppose that the measured data are available only in a short time interval.

The numerical results for the case that $k = 2$ and $T = 0.4$ are shown in Fig. 4.4, from which we see that the geometric information on D could still be captured, although the reconstructions look worse than those in Example 4.1. To numerically see the limit of shortness of the measuring time, we also test our method for $T = 0.3$ and $T = 0.15$. The numerical results for the pear-shaped domain are shown in Fig. 4.5. As the measuring time becomes short, the location of the inclusion can still be identified, but the shape is not well recovered.

Finally, let us mention that s of $G^{\Omega}_{(y,s)}$ was fixed in our numerical experiments. However, it is free to choose, and we can use this freedom to do the sampling in the following way. Let $\{y_{ij}\}$ be the sampling points given by (4.1). Define the order $\prec$ for two pairs of indices $(\ell,\, m)$ and $(\ell',\, m')$ of $y_{\ell,\,m}$ and $y_{\ell',\,m'}$ by

$$(\ell,\, m) \prec (\ell',\, m') \qquad \text{if either the case } \ell' > \ell \text{ or the case } \ell' = \ell \text{ and } m' > m.$$

Numerate these pairs $(\ell,\, m)$ of all $y_{\ell,\,m}$'s by this order so that $\{(\ell,\, m)\} = \{J\}$ with $J = 1,\, 2,\, \cdots, 640$. Consider a finite time series $\{\tilde{s}_J\}_{J=1}^{640} \subset (0,\, T)$ such that $\tilde{s}_1 < \tilde{s}_2 < \cdots < \tilde{s}_{640}$. At each $\tilde{s}_J$ we give a transient input as before and measure over $(\tilde{s}_J,\, \tilde{s}_J + \tau)$ with a small positive number τ. With these measurements, we can also reconstruct the inclusion by the sampling method as we did in [19] for the cavity case.

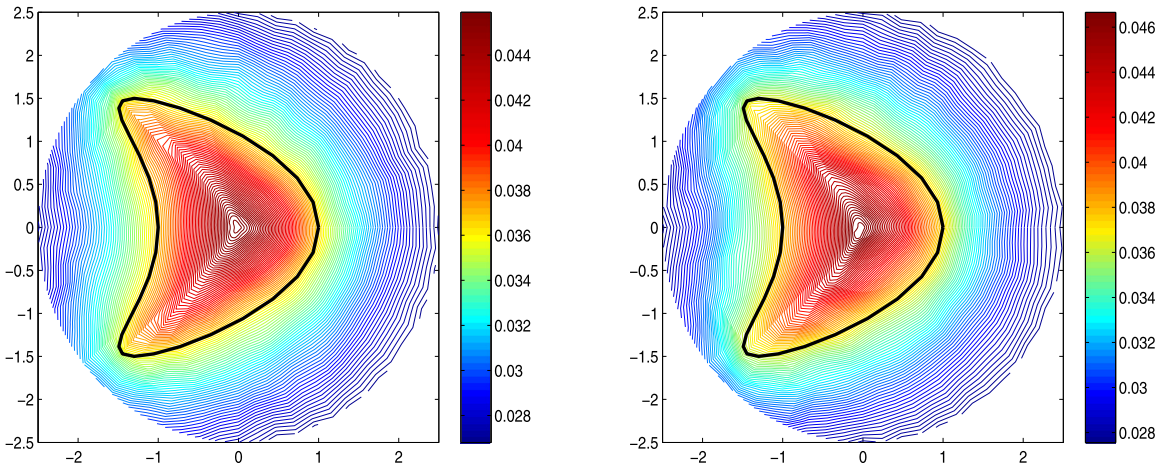

Fig. 4.1. Kite-shaped domain: $k = 0.5$ (left), $k = 2$ (right).

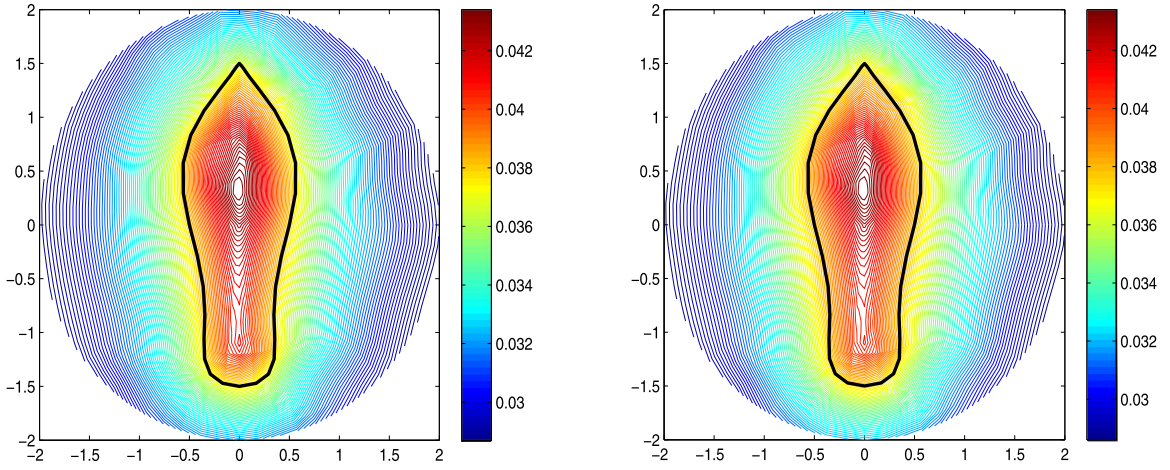

Fig. 4.2. Boat-shaped domain: $k = 0.5$ (left), $k = 2$ (right).

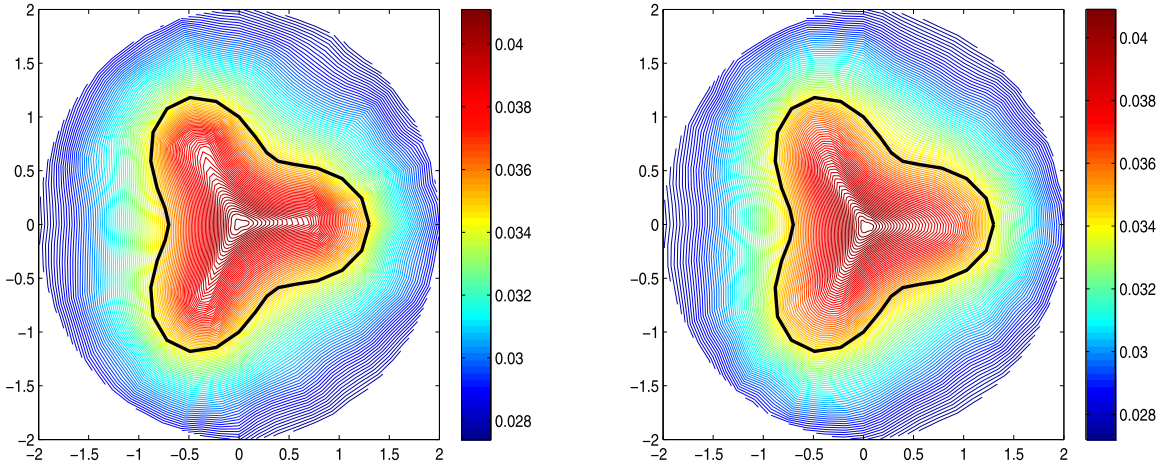

Fig. 4.3. Pear-shaped domain: $k = 0.5$ (left), $k = 2$ (right).

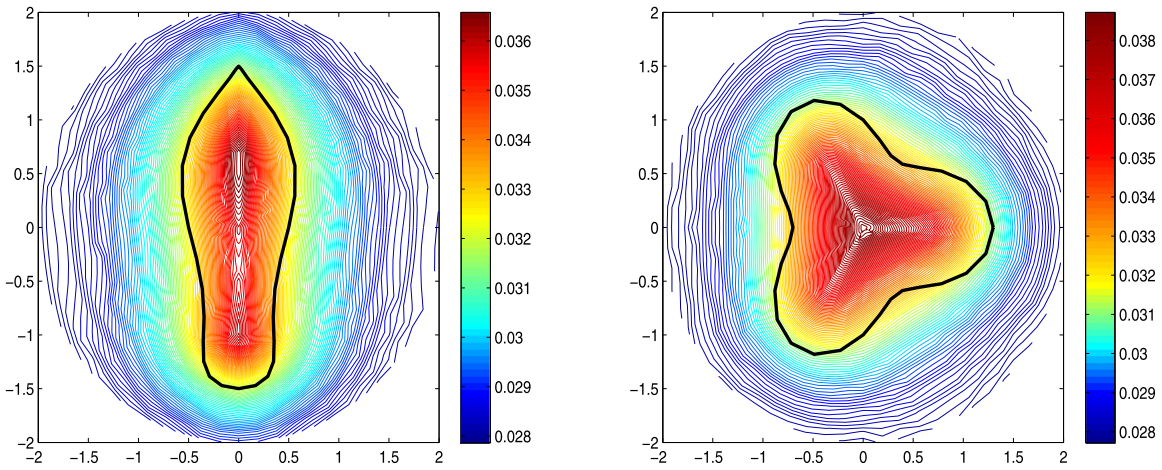

Fig. 4.4. Reconstructions for the case that $k = 2$ and $T = 0.4$.

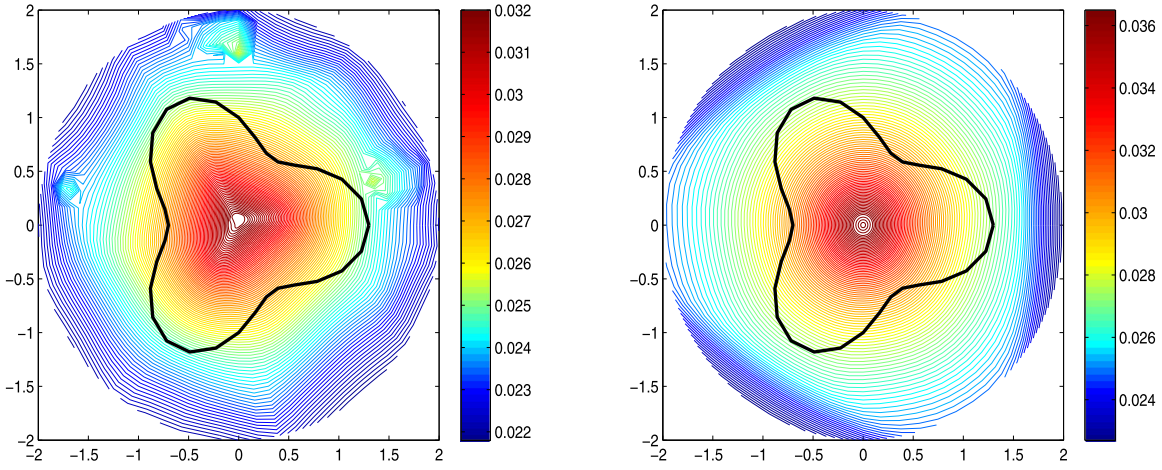

Fig. 4.5. Reconstructions of the pear-shaped domain: $T = 0.3$ (left) and $T = 0.15$ (right).

5. Concluding remarks

This paper continued our previous works and gave a further investigation of the sampling-type reconstruction method for identifying unknown inclusions inside the heat conductor. We first analyzed the solvability of the Neumann-to-Dirichlet map gap equation and established the relation of its solution to the Green function of an interior transmission problem for D_T. This naturally yielded a way of computing this Green function from the Neumann-to-Dirichlet map. A convergence result for noisy measurement data is also proved. Using the boundary integral equation method for the heat equation, we presented a numerical scheme for simulating the Neumann-to-Dirichlet map and the Green function $G^{\Omega}_{(y,\,s)}(x,\,t)$ which are known for the considered inverse problem. The discretized Neumann-to-Dirichlet map gap equation was solved by using the Tikhonov regularization method. The numerical experiments showed that our reconstruction method for the heat equation with unknown inclusions is effective and relatively stable to noise.

Acknowledgements

The authors would like to thank the referees for their careful reading and valuable suggestions, which made the paper much improved. This work is supported by National Natural Science Foundation of China (No. 11671082) and Qing Lan Project of Jiangsu Province.

References

[1] F. Cakoni, D. Colton, Qualitative Methods in Inverse Scattering Theory, Springer-Verlag, Berlin, 2006.
[2] R. Chapko, R. Kress, J.R. Yoon, On the numerical solution of an inverse boundary value problem for the heat equation, Inverse Probl. 14 (1998) 853–867.
[3] R. Chapko, R. Kress, J.R. Yoon, An inverse boundary value problem for the heat equation: the Neumann condition, Inverse Probl. 15 (1999) 1033–1046.

[4] M. Costabel, Boundary integral operators for the heat equation, Integral Equ. Oper. Theory 13 (1990) 498–552.
[5] M. Dawson, D. Borman, R.B. Hammond, D. Lesnic, D. Rhodes, A meshless method for solving a two-dimensional transient inverse geometric problem, Int. J. Numer. Methods Heat Fluid Flow 23 (2013) 790–817.
[6] Y. Daido, H. Kang, G. Nakamura, A probe method for the inverse boundary value problem of non-stationary heat equations, Inverse Probl. 23 (2007) 1787–1800.
[7] M. Di Cristo, S. Vessella, Stable determination of the discontinuous conductivity coefficient of a parabolic equation, SIAM J. Math. Anal. 42 (2010) 183–217.
[8] A. Elayyan, V. Isakov, On uniqueness of recovery of the discontinuous conductivity coefficient of a parabolic equation, SIAM J. Math. Anal. 28 (1997) 49–59.
[9] P. Gaitan, H. Isozaki, O. Poisson, S. Siltanen, J.P. Tamminen, Inverse problems for time-dependent singular heat conductivities: multi-dimensional case, Commun. Partial Differ. Equ. 40 (2015) 837–877.
[10] H. Harbrecht, J. Tausch, An efficient numerical method for a shape-identification problem arising from the heat equation, Inverse Probl. 27 (2011) 065013.
[11] H. Harbrecht, J. Tausch, On the numerical solution of a shape optimization problem for the heat equation, SIAM J. Sci. Comput. 35 (2013) A104–A121.
[12] H. Heck, G. Nakamura, H. Wang, Linear sampling method for identifying cavities in a heat conductor, Inverse Probl. 28 (2012) 075014.
[13] M. Ikehata, M. Kawashita, On the reconstruction of inclusions in a heat conductive body from dynamical boundary data over a finite time interval, Inverse Probl. 26 (2010) 095004.
[14] V. Isakov, K. Kim, G. Nakamura, Reconstruction of an unknown inclusion by thermography, Ann. Sc. Norm. Super. Pisa, Cl. Sci. (5) 9 (2010) 725–758.
[15] H. Isozaki, O. Poisson, S. Siltanen, J. Tamminen, Probing for inclusions in heat conductive bodies, Inverse Probl. Imaging 6 (2012) 423–446.
[16] G. Nakamura, S. Sasayama, Inverse boundary value problem for the heat equation with discontinuous coefficients, J. Inverse Ill-Posed Probl. 21 (2013) 217–232.
[17] G. Nakamura, H. Wang, Linear sampling method for the heat equation with inclusions, Inverse Probl. 29 (2013) 104015.
[18] G. Nakamura, H. Wang, Reconstruction of an unknown cavity with Robin boundary condition inside a heat conductor, Inverse Probl. 31 (2015) 125001.
[19] G. Nakamura, H. Wang, Numerical reconstruction of unknown Robin inclusions inside a heat conductor by a non-iterative method, Inverse Probl. 33 (2017) 055002.
[20] N.T. Thành, H. Sahli, D.N. Hào, Detection and characterization of buried landmines using infrared thermography, Inverse Probl. Sci. Eng. 19 (2011) 281–307.
[21] L. Yi, K. Kim, G. Nakamura, Numerical implementation for a 2-D thermal inhomogeneity through the dynamical probe method, J. Comput. Math. 28 (2010) 87–104.